Time-Course Change in Eye Shape and Development of Staphyloma in Highly Myopic Eyes

Tomotaka Wakazono,[1] Kenji Yamashiro,[1,2] Masahiro Miyake,[1] Masayuki Hata,[1] Manabu Miyata,[1] Akihito Uji,[1] Hideo Nakanishi,[1] Akio Oishi,[1] Hiroshi Tamura,[1] Sotaro Ooto,[1] and Akitaka Tsujikawa[1]

[1]Department of Ophthalmology and Visual Sciences, Kyoto University Graduate School of Medicine, Kyoto, Japan
[2]Department of Ophthalmology, Japanese Red Cross Otsu Hospital, Otsu, Japan

Correspondence: Kenji Yamashiro, Department of Ophthalmology and Visual Sciences, Kyoto University Graduate School of Medicine, 54 Kawahara, Shogoin, Sakyo, Kyoto 606-8507, Japan; yamashro@kuhp.kyoto-u.ac.jp.

Submitted: May 14, 2018
Accepted: October 18, 2018

Citation: Wakazono T, Yamashiro K, Miyake M, et al. Time-course change in eye shape and development of staphyloma in highly myopic eyes. *Invest Ophthalmol Vis Sci*. 2018;59:5455–5461. https://doi.org/10.1167/iovs.18-24754

Purpose. To quantitatively assess the posterior pole shape change in highly myopic eyes and to investigate the factors determining the speed of shape change.

Methods. Local curvature of the Bruch's membrane on the optical coherence tomography image was measured at intervals of 1 μm, and the mean curvature and curvature variance were calculated for 1094 eyes with an axial length of ≥26 mm. Speed of shape change was calculated using two points of mean curvature and curvature variance, and compared according to age, sex, axial length, and baseline eye shape.

Results. The posterior pole shape of females changed significantly greater than males ($P < 0.01$). Protruding change through the mean curvature was the greatest in the eyes with an axial length of ≥28 mm and <29 mm, while undulating change through the curvature variance became greater with axial length elongation in the eyes with an axial length of <29 mm and showed similar change in the eyes with an axial length of ≥29 mm. The eyes with a flatter shape at baseline tended to show a slow shape change, whereas those with moderate shape deformation at baseline showed faster shape change.

Conclusions. Quantitative evaluation of posterior pole eye shape clearly demonstrated significant time-dependent protruding and undulating changes in highly myopic eyes. Sex, axial length, and baseline posterior pole eye shape significantly affected speed of the posterior pole shape change. Our findings will facilitate risk assessment of staphyloma-associated complications in highly myopic eyes through measurement of speed of the posterior pole shape change.

Keywords: axial length, high myopia, optical coherence tomography, posterior pole eye shape, staphyloma

The prevalence of high myopia is increasing worldwide.[1–5] Because high myopia is associated with various ocular complications leading to severe visual impairment, more patients may be at risk of low vision or blindness in the near future. Many of these complications develop in association with posterior staphyloma in highly myopic eyes.[6–15] Studies on posterior staphyloma or posterior pole eye shape are needed to understand the mechanisms by which vision-threatening complications develop in high myopia, and preventive measures need to be identified. However, studies on staphyloma progression are limited, and time-course change of the posterior pole shape in highly myopic eyes has not been thoroughly investigated.

In eyes with posterior staphyloma, the posterior pole shape is characterized by protrusion in the posterior direction, and is sometimes accompanied by an undulated surface. In previous studies, we have shown that the protruding change and undulated change in the posterior pole shape can be quantitatively evaluated through using optical coherence tomography (OCT) images.[16–18] Quantitative evaluation of the posterior pole shape revealed that the eyes with myopic choroidal neovascularization (mCNV), myopic traction maculopathy, and chorioretinal atrophy had a unique characteristic shape; and the eyes with staphyloma and those without staphyloma could be clearly distinguished through quantitative measures of the curvature of OCT images.[16] In addition, quantitative analysis of OCT images could predict the occurrence of myopic traction maculopathy in highly myopic eyes.[17] Furthermore, quantitative evaluation of the posterior pole through OCT imaging was useful for epidemiologic cohort studies on staphyloma.[18] In the present study, we evaluated speed of the posterior pole shape change at two time points of OCT examination in highly myopic eyes, and investigated its association with sex, age, axial length, and baseline posterior pole shape.

Materials and Methods

We retrospectively examined 1173 eyes from 730 consecutive patients whose eyes with axial length of ≥26 mm underwent 9-mm cross scans of spectral-domain OCT (RS-3000; Nidek, Gamagori, Japan) with the fovea at the center, at least two times with interval of at least 1 year at the Department of Ophthalmology in Kyoto University Hospital (Kyoto, Japan) from April 2010 through November 2016. Only patients aged

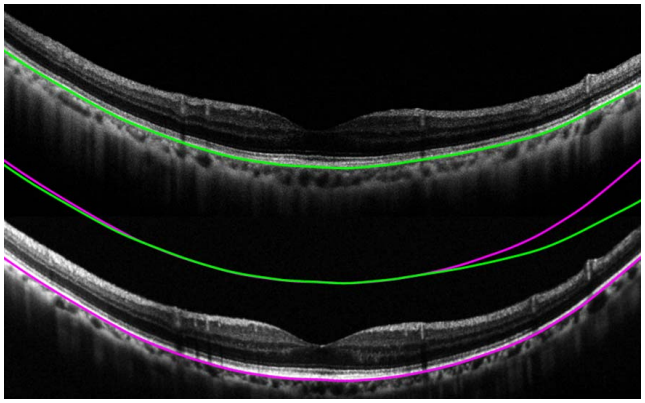

FIGURE 1. An example of the eyes used for the analysis is shown. The *upper image* shows the OCT image at the first examination with mean curvature of 6.17×10^{-5} μm^{-1} and curvature variance of 1.06×10^{-9} μm^{-2}. The *green line* shows the Bruch's membrane line in the OCT image. The *lower image* shows the OCT image at the last examination with mean curvature of 7.50×10^{-5} μm^{-1} and curvature variance of 1.13×10^{-9} μm^{-2} for the same eye. The *purple line* shows the Bruch's membrane line in the OCT image. The *middle image* clearly shows the curvature change from the first examination (*green line*) to the last examination (*purple line*).

≥20 years were included. Among the 1173 eyes, 79 were excluded because of insufficient quality of OCT images to precisely plot the Bruch's membrane line and a total of 1094 eyes from 698 patients were used for the analysis. For each eye, scans acquired at two time points with maximum interval were selected for the analysis. The axial length was measured using partial coherence interferometry or ultrasound. The axial length at the closest day from the time point of the first scan and age of the patient at the first scan were used for the analysis. The Ethics Committee at Kyoto University Graduate School of Medicine approved this study, which was conducted in accordance with the tenets of the Declaration of Helsinki.

The local curvature of the Bruch's membrane on the OCT image was evaluated at intervals of 1 μm using custom software RetinaView (Canon, Tokyo, Japan), as our previously established work.[16–18] The mean absolute curvature and variance of absolute curvature were calculated for each eye to evaluate the protruding shape change and undulating shape change, respectively (Fig. 1). The speed of the mean curvature change was calculated as the difference between the mean curvatures at the last and the first examinations, divided by the examination interval. The speed of the curvature variance change was calculated as the difference between variances of curvature at the last and the first examinations, divided by the examination interval.

Examples of the Bruch's membrane lines in OCT images are shown as curved lines in Figure 2. The curvature at each point is represented by the length of arrows in order to explain the concept of curvature analysis. The longer arrow indicates steeper curvature compared with the shorter arrow, and dotted lines were drawn to help readers easily comprehend the curvature. (A) A representative eye with continuously weak curvature. The mean curvature of this eye is calculated by averaging the curvatures measured at 1-μm intervals. Because the curvature severity represented by the length of the arrow at several points is the same for all arrows in this eye, the mean curvature is calculated as the length of a single arrow. The curvature variance of this eye is calculated using the curvatures measured at 1-μm intervals. The curvature is represented by the arrow length at several points, and the length is the same in all arrows in this eye; hence, the curvature variance is

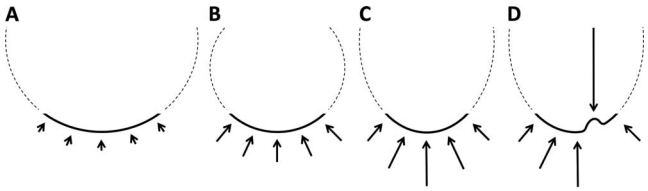

FIGURE 2. Examples of the Bruch's membrane lines in OCT images are shown with *curved lines*. The curvature at each point is represented by the length of *arrows* in order to explain the concept of the curvature analysis. *Longer arrow* indicates steeper curvature, and *dotted lines* allow the readers to easily comprehend the curvature. (**A**) A representative eye with continuously weak curvature. (**B**) A representative eye with greater continuous curvature. (**C**) A representative eye with steeper curvature at the bottom around the fovea. (**D**) A representative eye with steeper curvature at the bottom around the fovea together with undulated surface.

calculated as 0. (B) A representative eye with constant curvature. Because the curvature is greater, the drawing shows longer arrows. In this eye, the mean curvature is calculated by averaging the curvatures measured at 1-μm intervals. Because the curvature is represented by a greater length of the arrows at several points, and the length is the same in all arrows in this eye, the mean curvature is calculated based on the length of the longer arrows. Because the length of all arrows is the same in this eye, the curvature variance is calculated as 0. (C) A representative eye with steeper curvature at the bottom around the fovea. According to the curvature, the drawing shows arrows of greater length at the bottom and those of shorter length around the edge. The mean curvature of this eye is represented by the average length of all the arrows. The curvature variance calculated using all the arrows is greater than that of the eye with constant curvature. (D) A representative eye with steeper curvature at the bottom around the fovea, with undulated surface. The mean curvature calculated through using all the arrows is greater since there are many long arrows indicating steep curvature, and the curvature variance calculated through using all the arrows is greater because this eye has both short arrows and long arrows.

In the OCT image of the eye, the change between the curved line drawn in (A) and the curved line in (B) in 500 days, represents the amount of change of the mean curvature calculated as the difference between the length of the short arrow in (A) and the length of the longer arrow in (B). The speed of the mean curvature change per day is calculated by dividing the change amount by 500, and that of the change per year is calculated by multiplying the speed per day by 365. Because the variance of absolute curvature is 0 in both eyes, the speed of the curvature variance change is calculated as 0.

In the OCT image of the eye, the change between the curved line drawn in (C) and the curved line in (D) in 500 days, represents the amount of change of the mean curvature calculated as the difference between the average length of the arrow in (C) and the average length of the arrow in (D). The speed of the mean curvature change per day is calculated by dividing the change amount by 500, and that of the change per year can be calculated by multiplying the change speed per day by 365. The change amount of the curvature variance is represented by the difference between the variance of the arrow length in (C) and the variance of the arrow length in (D). The speed of the curvature variance change per day is calculated by dividing the change amount by 500, and that of the change per year can be calculated by multiplying the speed per day by 365.

Table 1. Characteristics of the Study Population

No. of eyes	1094
Sex,* male:female	245:453
Axial length, mm	28.47 ± 1.88
Age,* y	63.4 ± 13.8
Mean absolute curvature at the first examination, $\times 10^{-5}$ μm^{-1}	10.41 ± 5.06
Variance of absolute curvature at the first examination, $\times 10^{-9}$ μm^{-2}	4.87 ± 4.49

Data are presented as means ± SDs where applicable.
* If both eyes were analyzed in one patient, the data for the right eye of the patient were used.

The speed of change of the mean curvature and curvature variance were compared between males and females using the unpaired *t*-test. Moreover, the speed was compared among six age groups: age of <40 years, -(40); ≥40 and <50, 40-(50); ≥50 and <60, 50-(60); ≥60 and <70, 60-(70); ≥70 and <80, 70-(80); and ≥80, 80-; and five axial length groups: eyes with axial length of ≥26 mm and <27 mm, 26-(27); ≥27 mm and <28 mm, 27-(28); ≥28 mm and <29 mm, 28-(29); ≥29 mm and <30 mm, 29-(30); and ≥30 mm, 30-, using ANOVA and Tukey's test. In addition, the speed was compared among five groups of mean curvature at the first examination: $<7.5 \times 10^{-5}$ μm^{-1} (-[7.5]), $\geq 7.5 \times 10^{-5}$ μm^{-1} and $<10.0 \times 10^{-5}$ μm^{-1} (7.5-[10]), $\geq 10.0 \times 10^{-5}$ μm^{-1} and $<12.5 \times 10^{-5}$ μm^{-1} (10-[12.5]), $\geq 12.5 \times 10^{-5}$ μm^{-1} and $<15.0 \times 10^{-5}$ μm^{-1} (12.5-[15]), and $\geq 15.0 \times 10^{-5}$ μm^{-1} (15-); and five groups of curvature variance at the first examination: $<2.5 \times 10^{-9}$ μm^{-2} (-[2.5]), $\geq 2.5 \times 10^{-9}$ μm^{-2} and $<5.0 \times 10^{-9}$ μm^{-2} (2.5-[5]), $\geq 5.0 \times 10^{-9}$ μm^{-2} and $<7.5 \times 10^{-9}$ μm^{-2} (5-[7.5]), $\geq 7.5 \times 10^{-9}$ μm^{-2} and $<10.0 \times 10^{-9}$ μm^{-2} (7.5-[10]), and $\geq 10.0 \times 10^{-9}$ μm^{-2} (10-), using ANOVA and Tukey's test. All statistical analyses were performed using Statistical Package for the Social Sciences (SPSS, version 24.0; IBM, New York, NY, USA). A *P* value of <0.05 was considered as statistically significant.

Results

Characteristics of the study population are shown in Table 1. The mean age was 63.4 ± 13.8 years, and the mean axial length was 28.47 ± 1.88 mm. The interval between the two time points of OCT examination was 1098.7 ± 561.2 days (366–2429 days, Fig. 3). In the whole study population, mean speed of the mean curvature change or the protruding change was 1.45×10^{-6} (μm^{-1}/y), and mean speed of the curvature variance change or the undulating change was 1.73×10^{-10} (μm^{-2}/y). Speeds of both the mean curvature change (Fig. 4A) and curvature variance change (Fig. 4B) were significantly higher in females than males (Table 2, $P = 9.97 \times 10^{-3}$ and 7.26×10^{-4}, respectively).

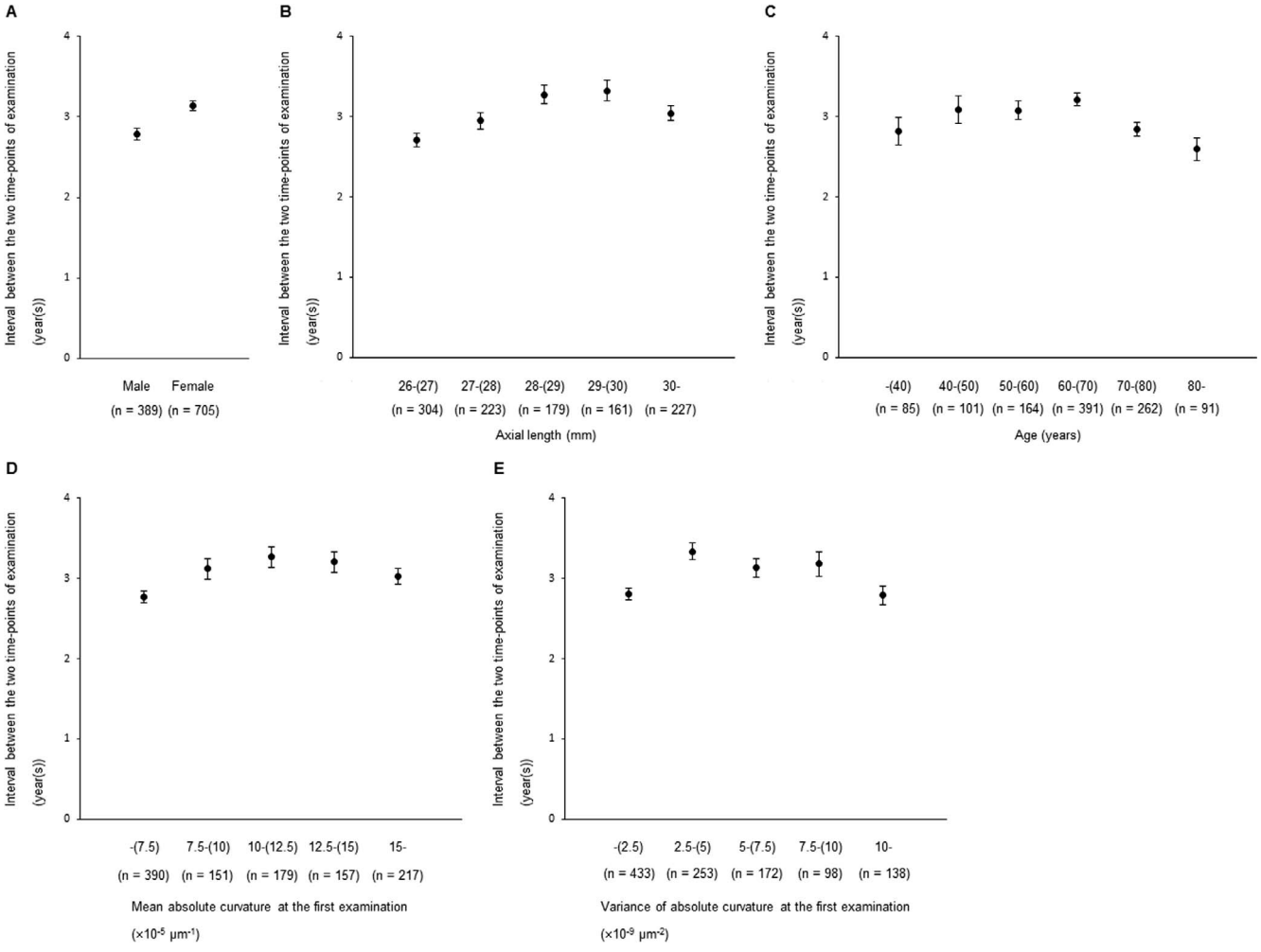

Figure 3. Interval according to the sex (**A**), axial length (**B**), age (**C**), mean absolute curvature at first examination (**D**), and variance of the absolute curvature at first examination (**E**). *Plots* show the means, and *error bars* show the standard errors.

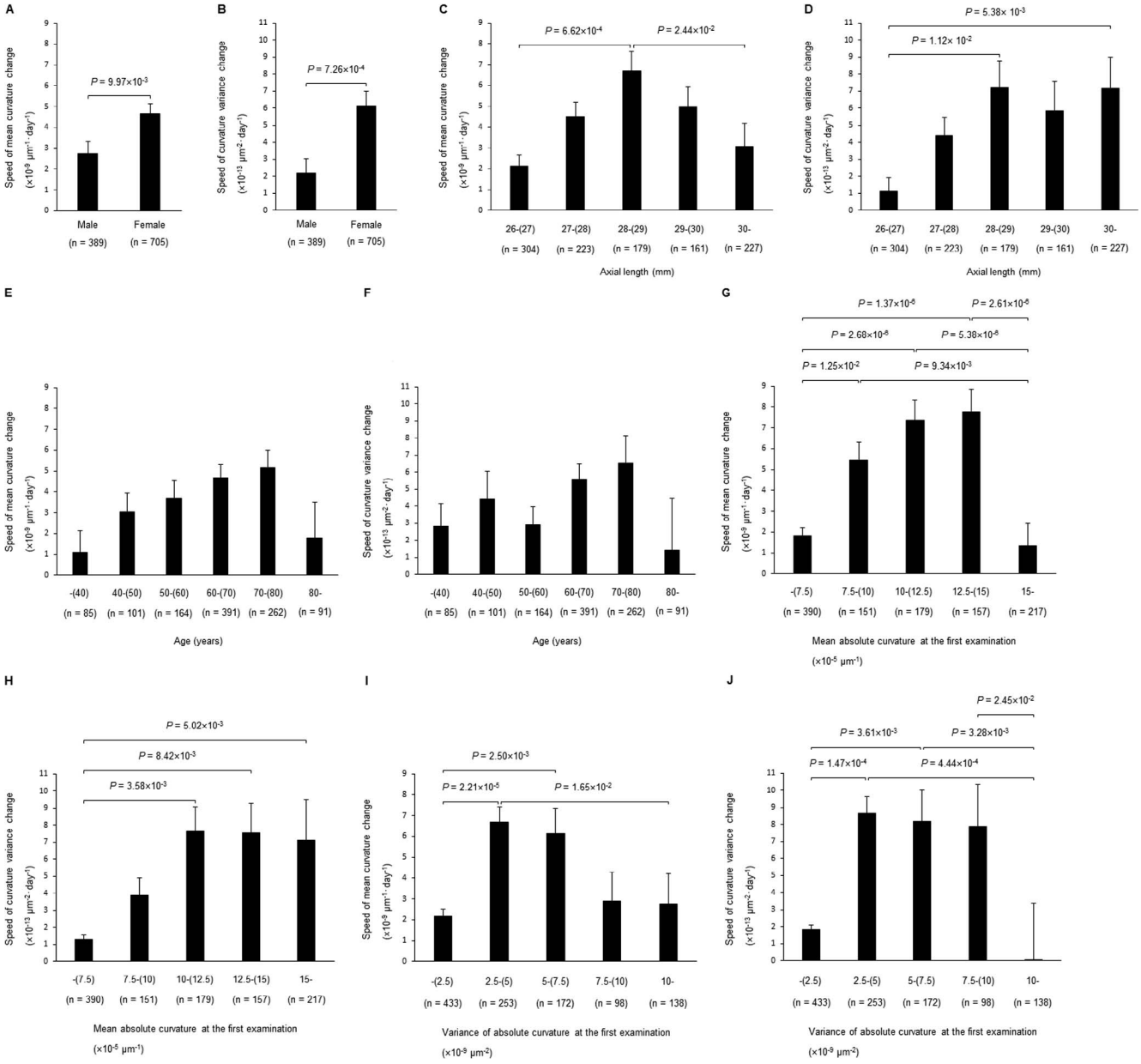

Figure 4. Speeds of the mean curvature change and the curvature variance change according to the sex (**A**, **B**), axial length (**C**, **D**), age (**E**, **F**), initial mean absolute curvature (**G**, **H**), and initial variance of the absolute curvature (**I**, **J**). *Bar graphs* show the means, and *error bars* show the standard errors. Both speeds were significantly higher in females than in males (**A**, **B**, $P = 9.97 \times 10^{-3}$ and 7.26×10^{-4}, respectively). With regard to the axial length, speeds of the mean curvature change (**C**) and the curvature variance change (**D**) were significantly different through ANOVA ($F_{4,1089} = 4.704$ and 4.136, $P = 9.12 \times 10^{-4}$ and 2.49×10^{-3}, respectively). With regard to the age, speed of the mean curvature change was significantly different through ANOVA (**E**, $F_{5,1088} = 2.472$, $P = 3.08 \times 10^{-2}$), but the curvature variance was not (**F**, $F_{5,1088} = 1.476$). With regard to the initial mean curvature, speed of the mean curvature change (**G**) and the curvature variance change (**H**) were significantly different through ANOVA ($F_{4,1089} = 14.167$ and 5.524, $P = 2.82 \times 10^{-11}$ and 2.10×10^{-4}, respectively). With regard to the initial curvature variance, speed of the mean curvature change (**I**) and the curvature variance change (**J**) were significantly different through ANOVA ($F_{4,1089} = 7.623$ and 8.616, $P = 4.67 \times 10^{-6}$ and 7.59×10^{-7}, respectively). *P* values of <0.05 by Tukey's test are shown in each graph.

Characteristics associated with axial length are shown in Table 3. Speed of the mean curvature change was significantly different among the five axial length groups ($F_{\text{degree of freedom between groups, degree of freedom within groups}} = F_{4,1089} = 4.704$, $P = 9.12 \times 10^{-4}$), with gradual increase from the eyes with axial length of ≥26 mm and <27 mm to the eyes with axial length of ≥28 mm and <29 mm (Fig. 4C, $P = 6.62 \times 10^{-4}$), and subsequent decrease in the eyes with axial length of ≥30 mm ($P = 2.44 \times 10^{-2}$). In contrast to speed of the mean curvature change, speed of the curvature variance change gradually increased from the eyes with axial length of ≥26 mm and <27 mm to the eyes with axial length of ≥28 mm and <29 mm (Fig. 4D, $P = 1.12 \times 10^{-2}$), and then maintained the high speed up to axial length of ≥30 mm ($P = 5.38 \times 10^{-3}$).

Characteristics associated with age are shown in Table 4. Speed of mean curvature change was significantly different among the six age groups, as indicated by ANOVA ($F_{5,1088} = 2.472$, $P = 3.08 \times 10^{-2}$). It increased gradually with age until the age of 80, and then decreased (Fig. 4E). However, the Tukey's test did not detect statistically significant difference in

Table 2. Characteristics Associated With Sex

Characteristic	Sex	
	Male	Female
No. of eyes	389	705
Axial length, mm	28.15 ± 1.88	28.65 ± 1.86
Age,* y	62.2 ± 13.8	64.0 ± 13.8
Mean absolute curvature at the first examination, $\times 10^{-5}$ μm^{-1}	8.51 ± 4.60	11.45 ± 5.00
Variance of absolute curvature at the first examination, $\times 10^{-9}$ μm^{-2}	3.59 ± 3.89	5.58 ± 4.64

Data are presented as means ± SDs where applicable.
* If both eyes were analyzed in one patient, the data for the right eye of the patient were used.

speed, in any age group. The speed of the curvature variance change also increased gradually until the age of 80 (Fig. 4F), but the increase was not statistically significant.

The baseline posterior pole shape affected the subsequent speed of the mean curvature change and curvature variance change. Characteristics associated with the mean absolute curvature at first examination are shown in Table 5. The speed of the mean curvature change gradually increased from the flatter eyes with the initial mean curvature of $<7.5 \times 10^{-5}$ μm^{-1} to the eyes with greater curvature of $\geq 12.5 \times 10^{-5}$ μm^{-1} and $<15.0 \times 10^{-5}$ μm^{-1} (Fig. 4G, $P = 1.37 \times 10^{-6}$). However, the eyes with greater curvature of $\geq 15.0 \times 10^{-5}$ μm^{-1} showed a slower speed of the curvature change. In contrast to the mean curvature, speed of the curvature variance change gradually increased from the flatter eyes with initial mean curvature of $<7.5 \times 10^{-5}$ μm^{-1} to the eyes with greater curvature of $\geq 10.0 \times 10^{-5}$ μm^{-1} and $<12.5 \times 10^{-5}$ μm^{-1} (Fig. 4H, $P = 3.58 \times 10^{-3}$), and then maintained the high speed until the greater curvature was $\geq 15.0 \times 10^{-5}$ μm^{-1} ($P = 5.02 \times 10^{-3}$).

In addition, baseline variance of the absolute curvature affected subsequent speed of the mean curvature change and curvature variance change. Characteristics associated with a variance of the absolute curvature at first examination are shown in Table 6. The speed of the mean curvature change was significantly higher in the eyes with initial curvature variance of $\geq 2.5 \times 10^{-9}$ μm^{-2} and $<5.0 \times 10^{-9}$ μm^{-2}, and $\geq 5.0 \times 10^{-9}$ μm^{-2} and $<7.5 \times 10^{-9}$ μm^{-2} (Fig. 4I, $P = 2.21 \times 10^{-5}$ and 2.50×10^{-3}, respectively). The eyes with greater curvature variance at initial examination did not show notably high speed. Speed of the curvature variance change showed a similar pattern (Fig. 4J). It was significantly higher in the eyes with initial curvature variance of $\geq 2.5 \times 10^{-9}$ μm^{-2} and $<5.0 \times 10^{-9}$ μm^{-2}, and $\geq 5.0 \times 10^{-9}$ μm^{-2} and $<7.5 \times 10^{-9}$ μm^{-2}, than in the eyes with initial curvature variance of $<2.5 \times 10^{-9}$ μm^{-2} ($P = 1.47 \times 10^{-4}$ and 3.61×10^{-3}, respectively) and $\geq 10.0 \times 10^{-9}$ μm^{-2} ($P = 4.44 \times 10^{-4}$ and 3.28×10^{-3}, respectively).

Discussion

Although the progression of posterior staphyloma and/or posterior pole eye shape change could significantly affect development of vision-threatening complications in highly myopic eyes, there has been limited research involving quantitative evaluation of the eye shape change at the posterior pole. The present study quantitatively demonstrated that the posterior pole shape significantly changed with time in highly myopic eyes. The mean curvature significantly increased, suggesting that the shape became more protruded with time; and, the curvature variance significantly increased, suggesting that the shape became more undulated with time. In this study, quantitative analysis suggested that speed of the posterior pole shape change was approximately 1.7- to 2.8-fold higher in females than in males, both for the protruding change and the undulating change. These differences are in agreement with previous reports of the predominance of myopic macular complications in female patients with high myopia.[16,19] Quantitative evaluation of speed of the eye shape change at the posterior pole has potential to predict occurrence of vision-threatening complications in highly myopic eyes, and would be useful in understanding the factors that affect speed of the eye shape change at the posterior pole and, thus, in developing preventive methods for such complications.

There was a clear difference in effect of the axial length on the protruding change and undulating change in highly myopic eyes. Speed of the protruding change was highest in the eyes with axial lengths of ≥28 mm and <29 mm, and decreased as the axial length became shorter or longer. In contrast, speed of the undulating change increased from the eyes with axial length of <27 mm to the eyes with axial length of ≥28 mm and <29 mm. The eyes with axial length of ≥29 mm showed similar speed to that of the eyes with axial length of ≥28 mm and <29 mm. Thus, we need to pay attention to both protruding and undulating changes in highly myopic eyes with axial length of <29 mm, while undulating change in the eyes with axial length of ≥29 mm need more attention. With regard to association between the age and speed of the posterior pole shape change, it was evident that both the protruding change and undulating change progressed faster with age until the age of 80, and subsequently slowed. Close attention should be paid to the posterior pole shape change in the high myopic patients until they attain the age of 80 years.

The baseline shape of the posterior pole significantly affected speed of the posterior pole shape change in highly myopic eyes. The eyes with flatter shape at baseline tended to change shape slowly, and the eyes with moderate shape deformation at baseline tended to show quicker eye shape change. The finding of low speed of the mean curvature change in the eyes with baseline mean curvature of $>15.0 \times 10^{-5}$ μm^{-1} would suggest that the maximum mean curvature for the most highly myopic eyes is approximately 15.0×10^{-5} μm^{-1}; whereas, the finding of low speed of the curvature

Table 3. Characteristics Associated With Axial Length

Characteristic	Axial length, mm				
	26-(27)	27-(28)	28-(29)	29-(30)	30-
No. of eyes	304	223	179	161	227
Sex,* male:female	89:106	50:89	34:80	30:70	42:108
Age,* y	61.8 ± 13.8	61.8 ± 16.1	65.4 ± 12.8	63.6 ± 13.6	65.2 ± 12.1
Mean absolute curvature at the first examination, $\times 10^{-5}$ μm^{-1}	6.18 ± 3.06	8.48 ± 3.77	11.07 ± 4.13	12.73 ± 3.76	15.80 ± 3.55
Variance of absolute curvature at the first examination, $\times 10^{-9}$ μm^{-2}	1.99 ± 2.21	3.31 ± 3.12	5.03 ± 4.16	6.42 ± 4.22	9.05 ± 4.72

Data are presented as means ± SDs where applicable.
* If both eyes were analyzed in one patient, the data for the right eye of the patient were used.

Table 4. Characteristics Associated With Age

Characteristic	Age, y					
	-(40)	40-(50)	50-(60)	60-(70)	70-(80)	80-
No. of eyes	85	101	164	391	262	91
Sex,* male:female	17:34	27:34	36:63	83:151	65:120	17:51
Axial length, mm	27.91 ± 1.61	28.23 ± 1.64	28.19 ± 1.92	28.69 ± 1.98	28.63 ± 1.87	28.39 ± 1.78
Mean absolute curvature at the first examination, $\times 10^{-5}$ μm^{-1}	6.12 ± 2.95	7.76 ± 3.82	8.42 ± 4.41	10.73 ± 4.72	12.47 ± 4.76	13.62 ± 5.74
Variance of absolute curvature at the first examination, $\times 10^{-9}$ μm^{-2}	1.73 ± 1.90	2.99 ± 3.33	3.11 ± 3.05	5.01 ± 4.40	6.31 ± 4.37	8.35 ± 5.96

Data are presented as means ± SDs where applicable.
* If both eyes were analyzed in one patient, the data for the right eye of the patient were used.

variance change in the eyes with baseline curvature variance of $>10.0 \times 10^{-9}$ μm^{-1} would suggest that the maximum curvature variance for the most highly myopic eyes is approximately 10.0×10^{-9} μm^{-1}.

Speed of the mean curvature change varied largely from 9.17×10^{-8} μm^{-1} per year in male subjects with axial length of ≥26 mm and <27 mm and age of <40 years ($n = 9$) to 4.64×10^{-6} μm^{-1} per year in female subjects with axial length of ≥28 mm and <29 mm and age of ≥70 and <80 years ($n = 40$). In our previous study, we demonstrated that each complication of highly myopic eyes was characterized by the unique posterior pole shape.[16] Moreover, the mean curvature was $(8.61 \pm 4.2) \times 10^{-5}$ μm^{-1} in highly myopic eyes without complications, $(11.27 \pm 3.01) \times 10^{-5}$ μm^{-1} in the eyes with myopic choroidal neovascularization (mCNV), and $(14.39 \pm 3.17) \times 10^{-5}$ μm^{-1} in the eyes with retinoschisis. Based on the differences in the characteristic mean curvatures, we could establish that eyes without complications would develop mCNV in 5.7 years, or retinoschisis in 12.5 years, at the highest speed of 4.64×10^{-6} μm^{-1} per year. Further longitudinal studies investigating the association between the eye shape at the posterior pole and development of vision-threatening complications are needed to allow accurate risk assessment of complications in highly myopic eyes. For example, mCNV develops in the eyes with moderate values of the mean curvature and curvature variance,[16] which suggests that the risk of developing mCNV would increase to some level and decrease thereafter as the curvature values increase. By estimating the rate of staphyloma progression, we can predict when the eye will be at high risk of developing mCNV and when at low risk of developing mCNV.

The limitations of the present study include its retrospective nature, and the small sample size. Our findings should be confirmed in prospective studies, and the role of the analyzing speed of posterior pole eye shape change in predicting development of complications in highly myopic eyes should be verified in large-scale prospective studies. The significant eye shape change at the posterior pole in the present study would suggest simultaneous significant change in the axial length in some highly myopic eyes. However, the axial length change would fall within the error margins of partial coherence interferometry or ultrasound measurement. The axial length change and the posterior eye shape change should be investigated in studies with longer observation periods. In addition, we evaluated the speed of the shape change under the assumption that the speed of the shape change is linear. Although our findings of no significant difference in speed according to the age would suggest that speed of the shape change was almost linear, the speed should be evaluated in a prospective study including several scheduled time points for the precise evaluation of speed. Moreover, close attention should be paid to the accuracy of the analysis of the curvature through OCT. OCT cannot capture the entire image of the posterior staphyloma in some highly myopic eyes. Speed of the curvature change in such eyes may be unique and, therefore, overlooked. A previous report indicated that OCT images tended to show flatter shape compared with that through magnetic resonance imaging,[20] and refractive error could affect the accuracy of the analysis of the curvature through OCT.[21] Because we analyzed the local curvature, the results of the analysis should be more precise than those through analyzing the whole OCT image. Analysis of curvature variance may have other weakness. For example, the curvature variance is calculated as 0 in the eyes with the posterior pole shape shown in Figures 2A and 2B, although the mean curvature is quite different. To overcome such weakness, both mean and variance values should be evaluated simultaneously.

In conclusion, the present study demonstrated through quantitative analysis that the eye shape at the posterior pole changed significantly with time, and speed of the posterior

Table 5. Characteristics Associated With Mean Absolute Curvature at the First Examination

Characteristic	Mean Absolute Curvature at the First Examination, $\times 10^{-5}$ μm^{-1}				
	-(7.5)	7.5-(10)	10-(12.5)	12.5-(15)	15-
No. of eyes	390	151	179	157	217
Sex,* male:female	128:108	33:63	36:79	22:81	26:122
Axial length, mm	27.01 ± 0.85	28.07 ± 1.10	28.67 ± 1.43	29.53 ± 1.63	30.47 ± 1.84
Age,* y	56.2 ± 15.1	61.4 ± 12.8	66.0 ± 11.9	68.2 ± 9.6	70.8 ± 10.1
Variance of absolute curvature at the first examination, $\times 10^{-9}$ μm^{-2}	1.26 ± 1.03	3.15 ± 1.41	4.73 ± 1.71	6.94 ± 2.47	11.19 ± 4.80

Data are presented as means ± SDs where applicable.
* If both eyes were analyzed in one patient, the data for the right eye of the patient were used.

Table 6. Characteristics Associated With Variance of Absolute Curvature at the First Examination

Characteristic	Variance of Absolute Curvature at the First Examination, $\times 10^{-9}$ μm^{-2}				
	-(2.5)	2.5-(5)	5-(7.5)	7.5-(10)	10-
No. of eyes	433	253	172	98	138
Sex,* male:female	135:128	50:112	33:78	10:58	17:77
Axial length, mm	27.17 ± 0.98	28.52 ± 1.46	29.25 ± 1.63	29.94 ± 1.70	30.47 ± 2.08
Age,* y	55.9 ± 14.6	64.9 ± 11.2	67.8 ± 10.9	69.4 ± 11.8	72.1 ± 9.4
Mean absolute curvature at the first examination, $\times 10^{-5}$ μm^{-1}	5.60 ± 1.93	10.50 ± 2.23	13.44 ± 2.53	15.57 ± 2.19	17.89 ± 3.40

Data are presented as means ± SDs where applicable.
* If both eyes were analyzed in one patient, the data for the right eye of the patient were used.

pole shape change varied depending on the sex, axial length, and baseline eye shape. The speed could be easily calculated with OCT images, and will be useful to predict the occurrence of complications in highly myopic eyes. Our findings on the associations between the speed of the posterior shape change and the age, sex, axial length, and initial eye shape, would be useful to predict the speed in each eye.

Acknowledgments

Disclosure: **T. Wakazono**, None; **K. Yamashiro**, None; **M. Miyake**, None; **M. Hata**, None, **M. Miyata**, None; **A. Uji**, Canon (R); **H. Nakanishi**, Tomey Corporation (F, R); **A. Oishi**, None; **H. Tamura**, None; **S. Ooto**, Nidek (R); **A. Tsujikawa**, Canon (F), Tomey Corporation (F), and Nidek (R)

References

1. Lin LL, Shih YF, Hsiao CK, Chen CJ. Prevalence of myopia in Taiwanese schoolchildren: 1983 to 2000. *Ann Acad Med Singapore*. 2004;33:27–33.
2. Vitale S, Sperduto RD, Ferris FL III. Increased prevalence of myopia in the United States between 1971–1972 and 1999–2004. *Arch Ophthalmol*. 2009;127:1632–1639.
3. Morgan IG, Ohno-Matsui K, Saw SM. Myopia. *Lancet*. 2012; 379:1739–1748.
4. Verkicharla PK, Ohno-Matsui K, Saw SM. Current and predicted demographics of high myopia and an update of its associated pathological changes. *Ophthalmic Physiol Opt*. 2015;35:465–475.
5. Holden BA, Fricke TR, Wilson DA, et al. Global prevalence of myopia and high myopia and temporal trends from 2000 through 2050. *Ophthalmology*. 2016;123:1036–1042.
6. Takano M, Kishi S. Foveal retinoschisis and retinal detachment in severely myopic eyes with posterior staphyloma. *Am J Ophthalmol*. 1999;128:472–476.
7. Benhamou N, Massin P, Haouchine B, Erqinay A, Gaudric A. Macular retinoschisis in highly myopic eyes. *Am J Ophthalmol*. 2002;133:794–800.
8. Baba T, Ohno-Matsui K, Futagami S, et al. Prevalence and characteristics of foveal retinal detachment without macular hole in high myopia. *Am J Ophthalmol*. 2003;135:338–342.
9. Oie Y, Ikuno Y, Fujikado T, Tano Y. Relation of posterior staphyloma in highly myopic eyes with macular hole and retinal detachment. *Jpn J Ophthalmol*. 2005;49:530–532.
10. Forte R, Cennamo G, Pascotto F, de Crecchio G. En face optical coherence tomography of the posterior pole in high myopia. *Am J Ophthalmol*. 2008;145:281–288.
11. Wu PC, Chen YJ, Chen YH, et al. Factors associated with foveoschisis and foveal detachment without macular hole in high myopia. *Eye (Lond)*. 2009;23:356–361.
12. Henaine-Berra A, Zand-Hadas IM, Fromow-Guerra J, García-Aguirre G. Prevalence of macular anatomic abnormalities in high myopia. *Ophthalmic Surg Lasers Imaging Retina*. 2013; 44:140–144.
13. Ohno-Matsui K. Proposed classification of posterior staphylomas based on analyses of eye shape by three-dimensional magnetic resonance imaging and wide-field fundus imaging. *Ophthalmology*. 2014;121:1798–1809.
14. Ohno-Matsui K, Lai TY, Lai CC, Cheung CM. Updates of pathologic myopia. *Prog Retin Eye Res*. 2016;52:156–187.
15. Guo X, Xiao O, Chen Y, et al. Three-dimensional eye shape, myopic maculopathy, and visual acuity: the Zhongshan Ophthalmic Center-Brien Holden Vision Institute High Myopia Cohort Study. *Ophthalmology*. 2017;124:679–687.
16. Miyake M, Yamashiro K, Akagi-Kurashige Y, et al. Analysis of fundus shape in highly myopic eyes by using curvature maps constructed from optical coherence tomography. *PLoS One*. 2014;9:e107923.
17. Wakazono T, Yamashiro K, Miyake M, et al. Association between eye shape and myopic traction maculopathy in high myopia. *Ophthalmology*. 2016;123:919–921.
18. Numa S, Yamashiro K, Wakazono T, et al. Prevalence of posterior staphyloma and factors associated with its shape in the Japanese population. *Sci Rep*. 2018;8:4594.
19. Asakuma T, Yasuda M, Ninomiya T, et al. Prevalence and risk factors for myopic retinopathy in a Japanese population: the Hisayama Study. *Ophthalmology*. 2012;119:1760–1765.
20. Kuo AN, McNabb RP, Chiu SJ, et al. Correction of ocular shape in retinal optical coherence tomography and effect on current clinical measures. *Am J Ophthalmol*. 2013;156:304–311.
21. Clark CA, Elsner AE, Konynenbelt BJ. Eye shape using partial coherence interferometry, autorefraction, and SD-OCT. *Optom Vis Sci*. 2015;92:115–122.

Investigative Ophthalmology & Visual Science